The Astronomical Journal, 132:420–432, 2006 July

OBSERVATIONS SUPPORTING THE EXISTENCE OF AN INTRINSIC MAGNETIC MOMENT INSIDE THE CENTRAL COMPACT OBJECT WITHIN THE QUASAR Q0957+561

Rudolph E. Schild,[1] Darryl J. Leiter,[2] and Stanley L. Robertson[3]
Received 2005 May 20; accepted 2006 April 3

ABSTRACT

Recent brightness fluctuation and autocorrelation analysis of time series data and microlensing size scales, seen in Q0957+561A and B, have produced important information about the existence and characteristic physical dimensions of a new nonstandard magnetically dominated internal structure contained within this quasar. This new internal quasar structure, which we call the Schild-Vakulik structure, can be consistently explained in terms of a new class of gravitationally collapsing solutions to the Einstein field equations that describe highly redshifted Eddington-limited magnetospheric eternally collapsing objects that contain intrinsic magnetic moments. Since observations of the Schild-Vakulik structure within Q0957+561 imply that this quasar contains an observable intrinsic magnetic moment, this represents strong evidence that the quasar does not have an event horizon.

Key words: accretion, accretion disks — black hole physics — gravitational lensing — magnetic fields — quasars: individual (Q0957+561)

1. INTRODUCTION

Analysis of gravitational microlensing observations of the quasar Q0957+561 (Schild & Vakulik 2003, hereafter SV03; Schild 2005b) has offered strong evidence for the existence of an intrinsic structure within this quasar that can only be explained by a nonstandard luminous quasar model consisting of a thin accretion disk whose interior is essentially empty of matter out to a luminous inner edge that resides at about 70 gravitational radii from the central compact object and that is also surrounded by an order of magnitude larger outer ring-shaped Elvis structure where the broad blueshifted emission lines are formed. While this nonstandard form of inner quasar structure (which we call the Schild-Vakulik structure) has been shown to have the remarkable property of being able to explain all of the observed features of Q0957+561 obtained from 24 years of gravitational microlensing study, the physical origin and interpretation of this exotic inner quasar structure have remained an unsolved mystery. During the same time period that the gravitational microlensing–based discovery of the Schild-Vakulik structure in quasar Q0957+561 occurred, a related new paradigm in astrophysics based on X-ray and radio astronomy data had begun to emerge. This new paradigm came in the form of five sequentially published papers that presented strong observational and theoretical evidence that both Galactic black hole candidates (GBHCs) and active galactic nuclei (AGNs) have observable intrinsic magnetic moments.

This latter discovery was revealed in the following manner: First, it was argued (Robertson & Leiter 2002) that the spectral state switch and quiescent luminosities of low-mass X-ray binaries, including GBHCs, can be well explained by a magnetic propeller effect that requires an intrinsically magnetized central object. Second, it was shown (Leiter & Robertson 2003; Robertson & Leiter 2003) that this result was consistent with the existence of a new class of gravitationally collapsing solutions of the Einstein field equations in general relativity that describe highly redshifted, magnetospheric eternally collapsing objects (MECOs) that do not have trapped surfaces leading to event horizons. These general relativistic MECO solutions were shown to emerge from the physical requirement that the structure and radiation transfer properties of the energy-momentum tensor on the right-hand side of the Einstein field equations for a collapsing object must contain equipartition magnetic fields that generate a highly redshifted Eddington-limited secular collapse process that satisfies the strong principle of equivalence (SPOE) requirement of timelike worldline completeness. Third, it was demonstrated (Robertson & Leiter 2004) that GBHCs and AGNs modeled as intrinsically magnetic MECOs can produce jets that emit radio-infrared luminosity correlated with mass and X-ray luminosity in a manner that correctly predicts the observed exponent, mass-scale invariant cutoff, and radio luminosity ratios of both GBHCs and AGNs. Finally, a full discussion of the entire observational and theoretical program for the MECO model of GBHCs and AGNs was published in the book *New Directions in Black Hole Research* (Robertson & Leiter 2005). In the following sections we show that the two different lines of research discussed above converge in a manner allowing the construction of a logical chain of observational and theoretical arguments that solves the mystery of the physical origin of the Schild-Vakulik structure observed within the quasar Q0957+561. In order to do this we use the MECO paradigm (discussed in detail in the appendices of Schild et al. [2005], an extended version of this paper) as a model to interpret the physical meaning of the gravitationally microlensed Schild-Vakulik structure seen in Q0957+561. In this context we show that the Schild-Vakulik structure actually represents the key observable dynamic signature of a 3.6 billion $M_{\odot}$ MECO acting as the central compact object in this quasar instead of a black hole. Hence, we are led to conclude that the observation of the Schild-Vakulik structure within Q0957+561 represents strong evidence that this quasar does not have an event horizon.

2. QUASAR STRUCTURE SIZE ESTIMATES FROM BRIGHTNESS TIME SERIES AUTOCORRELATION

The most accurate direct measurement available of the inner quasar size is in the long time series brightness data collected over many years to study the gravitational lens time delay and

[1] Center for Astrophysics, 60 Garden Street, Cambridge, MA 02138.
[2] Marwood Astrophysics Research Center, P.O. Box 7466, Charlottesville, VA 22906.
[3] Department of Physics, Southwestern Oklahoma State University, Weatherford, OK 73096.

microlensing. Evidence for the outer ring (Elvis 2000) structures in this data set has already been discussed by Schild (2005b) from analysis of the internally created repetitions seen in the long brightness record. In addition, an inner structure has also been discussed in Schild (2005b) and in previous references. Heretofore it has been discussed as the "luminous inner edge of the accretion disk," according to standard ideas of quasar structure dominated by a black hole surrounded by an accretion disk and perhaps outer clouds or Elvis outflow structures. However, more accurate recent numerical estimates of the size of the inner quasar structure of Q0957+561 have implied that its size is actually larger than previously estimated and for this reason better explained as the luminous ring expected at the magnetospheric radius of an empirical quasar model in which the central compact object in the quasar is dominated by the dynamic effects of an intrinsic magnetic propeller acting in this sensitive inner region. This improved, more accurate empirical quasar model for Q0957+561 has been found to be most consistently explained in the context of the recently discovered new class of gravitationally collapsing solutions to the Einstein field equations that describe compact gravitationally collapsing objects in terms of highly redshifted MECOs that do not have trapped surfaces leading to event horizons. In order to help the reader of this paper maintain the continuity and flow of the observational arguments that support the above conclusions, the specific details about the MECO model and the published articles associated with it have been put into a series of short appendices (Appendices 1–11 in Schild et al. 2005) and are referred to in the following paragraphs when needed in order to clarify the details of specific calculations associated with the observational data.

We now begin discussing the observational arguments referred to above by first noting that two manifestations of the dynamic inner structure of Q0957+561 A and B have been seen: (1) Direct autocorrelation calculations of the brightness record for the two image components have revealed an inner structure with an associated timescale of approximately 10 days (Schild 2005b). (2) Time delay calculations by several research groups have indicated that several time delays seem to be present. In particular, in addition to the now firmly established 417.1 day time delay (Colley et al. 2003), there is convincing evidence for lags of 404 days (Schild 1991; Thomson & Schild 1997) and 424 days (Pijpers 1997; Oscoz et al. 2001; Pelt et al. 1996). It is likely that these lags caused by internal structure are part of the reason why it has been so difficult to determine the cosmological time delay. Regarding (2) above, recall that the time delay controversy in the 1990s was probably a manifestation of quasar structure causing several lags to produce autocorrelation peaks that can also create spurious cross-correlation peaks. Recall that the difference between the 404 day concurrent time delay value (Schild 1991; Thomson & Schild 1997a, 1997b) and the erroneous Press et al. (1992) value of 534 days is exactly the 129 day value found as an autocorrelation peak illustrated in Figure 1 of Schild (2005b).

The existence of internal reflections/fluorescence as manifestations of internal quasar structure can easily be seen in the most recent brightness data for a different quasar, Q2237 (Einstein Cross).[4] Here we can recognize two distinct kinds of patterns in the brightness fluctuations of the four quasar images. Because the time delay between arrivals of the four images is essentially 0 days (see Vakulik 2006), the pattern of nearly identical fluctuations is a clear manifestation of intrinsic quasar brightness fluctuations. A nonintrinsic (microlensing) brightness fluctuation, peaking at JD $-$ 2,450,000 = 3500, is also seen for image B (yellow circles in the bottom figure on this Web page).

[4] Plotted at http://www.astrouw.edu.pl/~ogle/ogle3/huchra.html.

We now focus on the pattern of intrinsic brightness fluctuations. Local maxima are recognized at JD $-$ 2,450,000 = 2950, 3300, and 3700, with a possible first peak around 2500 poorly observed because of the poor OGLE III data sampling. The amplitudes and durations of these peaks, around 0.4 mag for 150 days, are comparable to the peaks and lags identified in Q0957+561 (Schild 2005b and earlier references). (Recall that the redshift of Q2237 is 1.69, about 20% higher than that of Q0957+561, so time dilation correction improves the comparison.)

Thus, the two gravitational lens systems with adequate data show a complex behavior whereby an intrinsic fluctuation is seen at multiple times, almost certainly betraying the existence of complex internal quasar structure that can confound time delay determination but that also provides important clues about the structure of the quasar. The previous generation of quasar models has ignored these structures and modeled the lensed quasars as solid accretion disks. This has produced, in all the numerous available simulations of Q2237 microlensing, the contradictions that an accretion disk small enough to allow interpretation of microlensing events as due to solar-mass stars produces brightness fluctuations with 2–3 mag amplitudes, and transverse velocity estimates 10 times larger than estimates from normal cosmology. These models have also produced the incorrect prediction of Wyithe et al. (2000) that now drives us away from the simple accretion disk model.

The Q0957+561 structures discussed above have durations and lags of order 150 days (observer's clock) or 60 proper days and are presumed to originate in the continuum-emitting regions associated with the Elvis structures (Schild 2005b). Shorter timescale lags, also caused by quasar internal structure, allow us to estimate the size of the inner edge of the accretion disk, using methodology and results from Schild (2005b). We assume that the cosmological time delay is 417.1 days (Colley et al. 2003) but that the internal quasar structure also produces lags at t_1 and t_2 following the initial impulse.

Thus, the impulse seen in the first-arriving A image correlates strongly with the second-arriving B image at lags of 417, $417 + t_1$, and $417 + t_2$ days. Of course, there should be strong correlation at $417 - t_2$ and $417 - t_1$ days due to secondary impulses contained in the A (first-arriving) image. Evidence for these lags shorter than the cosmological time delay has been reported by Schild & Thomson (1997a), who noted that "this calculation produces a broad maximum with an absolute peak for 387 day lag. Note that the calculation produces a number of peaks near 400 days, and that the peaks tend to have a uniform spacing of 16 days, which may correspond to an internal reflection within the inner quasar structure." Because the hot inner radius of the accretion disk is seen as the small brightness enhancement for two lags, corresponding to the ring radius and to the known inclination, we ask if the measured lags for the 404 and 424 day measured delays follow from the Schild (2005b) model and geometry in Q0957+561. The answer is an unqualified yes. The shortest lag, 7 days observed (i.e., 424−417 days), must correspond to the interaction (reflection/fluorescence) from the near side of the ring. Then the reflection from the far side must be at 13 days, which is both the lag measured (i.e., 417−404 days) and the lag predicted given the preferred case 1 geometry of Schild (2005b).

In other words, given the quasar inclination measured by Schild (2005b) from the Elvis structures and given one of the measured inner ring lags, we can predict the second (measured, 13 day) inner ring lag. This quasar structure and its interpretation is necessarily complicated because the effects of the solar-mass microlensing star must selectively magnify the two sides of the inner edge of the accretion disk differently at different times. While this produces complexity in interpretation, it also generates

information about the direction of motion of the microlensing star in the lens galaxy G1. Finally, from this complex chain of analysis of internal quasar structure, we determine the size of the luminous inner edge of the accretion disk. For the geometric factors of the model as determined above, the measured 424 and 404 day lags combined with a 417.1 day cosmological time delay (Colley et al. 2003) and correction for the 54° inclination of the quasar's pole from the line of sight (Schild 2005b) give a rather large value for the inner radius of the accretion disk of $(3.9 \pm 0.16) \times 10^{16}$ cm, where the error is estimated from the 1 day discreteness of the reported lags and the averaging of the two estimates from the above two lag determinations.

3. EMPIRICAL ESTIMATES OF THE THICKNESS OF THE HOT ANNULAR RING OBSERVED TO OCCUR AT THE INNER RADIUS OF THE ACCRETION DISK

The inner radius of the accretion disk (which is associated below with the MECO magnetospheric radius) is considered to be the smallest observable structure in the Q0957+561 quasar, and therefore, the rapid fluctuations observed by Colley & Schild (2003, hereafter CS03) are presumed to originate there. However, it is not yet clear by what mechanism the brightness fluctuations are produced. We consider that there are probably two processes contributing to the observed brightness patterns, microlensing and changes in the quasar structure. The most critical observations define a small size limit as seen in the CS03 data, which seem to demonstrate rapid brightness fluctuations of 1% amplitude and 12 hr duration in both the intrinsic quasar brightness fluctuations and in the microlensing.

We refer to the patterns of fluctuations shown in Figure 1 of CS03. There, on JD 2,449,701–2,449,705 we see a pattern of fluctuations that was seen in the first year of observations, in image A (*filled circles*), and after a 417 day time delay, seen in image B (*open circles*). The brightness trend seems to show convincingly that a pattern of intrinsic fluctuations was seen, with several brightness changes of approximately 1% with a timescale on the order of 12 hr. Thus, on day 1, the quasar appears to have declined in brightness by .017 mag in 0.43 days (*solid line fitted to the data points in the top panel*). Note that this must be an intrinsic quasar brightness fluctuation, because it is seen in both the first- and second-arriving images. In addition, microlensing fluctuations of comparable amplitude must exist, as again illustrated in Figure 1 of CS03. Referring to the data for JD 2,449,706, we can see from the many time-overlapping points that the quasar image brightness does not agree for this date, and the difference between the two observations for the same proper quasar time shows the profile illustrated in the bottom panel of Figure 1, where a microlensing event with a 12 hr timescale and 0.01 mag amplitude is detected. Because this profile must originate in microlensing, it would be expected to have a cusp-shaped profile unless the source structure is partially resolved, as seems to be observed here.

These simple amplitude and timescale estimates of microlensing and intrinsic quasar brightness changes are entirely compatible with previously published estimates, expressed as wavelet amplitude (Schild 1999), structure function (Colley & Schild 1999), and Fourier power spectrum (Thomson & Schild 1997). The wavelet fits to the A and B images separately (Schild 1999) measure the total amplitude in fluctuations independently of whether the fluctuations originate in intrinsic or microlensing variability. Nevertheless, the amplitudes measured for the A and B images are seen in Schild (1999, Fig. 8) to be of amplitude 1% on timescales of 2 days in the mean. The event in CS03 is exceptional by a factor of 4 in time, but this is of course a probable selection effect. The view that these most rapid low-amplitude fluctuations originate in the inner ring of the accretion disk produces a new view of the nature and origin of the quasar luminous signal and its microlensing.

If we adopt for the moment a model of the inner quasar where a disturbance of some kind, perhaps related to ingestion of a mass unit, is seen throughout the inner corona and the surrounding inner ring of the accretion disk, then we would expect to see the brightness enhancement signaling this event originating in the corona and later, after short lags of order days, when the event is seen in the nearer and then the farther sides of the inner ring of the accretion disk. Because each of these regions is microlensed independently and differently, it would be unsurprising if the microlensing has the same amplitudes and timescales for brightness fluctuations as the intrinsic brightness fluctuations, as observed. This important possible kind of microlensing is significantly different from the simpler view that the fluctuations are just caused by luminous elements crossing the caustic pattern originating in the lens galaxy (Gould & Miralda-Escude 1997; Rauch & Blandford 1991). However, our new approach requires the quasar to have very fine structure, whose size we now estimate.

3.1. *Estimation of Source and Microlensing Amplitudes and Their Timescales*

We estimate first the dimensions implied if we adopt the simple argument that for a significant brightness fluctuation to occur, something must be altering its physical properties, and therefore its luminosity, on a time sufficiently long that the observed coherence does not violate the principle of causality (meaning that the event is limited in size by the velocity of light). Thus, the proper scale of a quasar emitting region that coherently changes its luminosity by 5% (because dilution by the steady luminous emission of the large outer Elvis structures produces 80% of the observed quasar brightness, according to SV03) is at least as large as the light travel distance, ct. For the CS03 event with observed time 12 hr and proper time $12/2.41$ hr $= 5$ hr, the probable diameter of the coherent light-emitting region is 5.4×10^{14} cm. The numerical value of this length, estimated from the coherent brightness fluctuations, represents the radial thickness of the hot annular band at the inner radius of the accretion disk.

3.2. *Microlensing by Luminous Matter Passing behind Microlensing Cusps*

3.2.1. *Infall Case*

A second estimate of fluctuation source size comes from the model that the fluctuation is due to some luminous unit crossing a cusp originating in the lens galaxy. As already noted by Schild (1996), the cusp pattern would be produced by planetary-mass microlensing objects, which amplify the shear introduced by the stars also known to be in the lens galaxy, that are inferred to be not sufficient to be baryonic dark matter. This process has already been modeled by SV03, from which we can adopt some principal results. In SV03 the shear due to solar-mass stars is modeled as originating in a population with 0.1 $M_\odot$, but this adopted value is not expected to appreciably affect results since the planetary-mass population produces a very significantly finer cusp pattern with a factor of 10 larger optical depth. The model adopts standard values for cosmology and for the transverse velocity. A principal result of the model is that the microlensing brightness fluctuations that would be observed should be typically 0.01 mag on a timescale of 10 days (observer's clock), for an adopted thickness of the inner ring of 5.4×10^{14} cm and for 10^{-5} $M_\odot$ microlensing particles. This fluctuation time varies as the size of the emitting region and as the square of the microlens mass. Thus, the structure size scale estimated would be 10^{13} cm and the mass would

be $10^{-7}\,M_{\odot}$ for the somewhat resolved microlensing event found in CS03.

We find it unlikely that the Q0957+561 quasar has coherent structure on such small size scales, because the brightness fluctuations have no hint of it, although it is possible that an ingested mass unit powering the quasar does. Based on the above discussion, we adopt for now the more conservative conclusion that the observed rapid brightness fluctuations result from a local brightness change in the accretion disk seen at multiple epochs.

3.2.2. *Microlensing by Orbiting Luminous Material Generated by Magnetospheric Effects*

Another microlensing scenario was suggested by Gould & Miralde-Escude (1997) and previously by Rauch & Blandford (1991). In this scenario, orbiting blobs created in the magnetospheric ring region of the inner accretion disk, (e.g., like those described by the magnetically arrested disk [MAD] model [Igumenschev et al. 2003]) would pass behind the cusp pattern originating in the lens galaxy. However, to be visible, such blobs would necessarily have to have a luminosity comparable to that of the quasar coming from a volume with the diameter of the Sun. Furthermore, these luminous blobs would tend to make asymmetrical brightness profiles, characterized by successive brightness peaks only, contrary to the wavelet result by Schild (1999) that equal positive and negative fluctuations are found. Furthermore, the mechanism would produce highly periodic brightness effects not observed in any of the lensed quasar systems. Hence, we consider this mechanism not to be an important indicator of the quasar structure in Q0957+561 (for more details on this issue, see the theoretical analysis discussion in § 7 below).

4. STRUCTURE FUNCTION ESTIMATES INFERRED FROM LONG-TERM BRIGHTNESS FLUCTUATIONS

With the shortest timescale brightness fluctuations understood to be indicative of the thickness of the hot inner annulus of the accretion disk in Q0957+561, we consider next the properties of brightness fluctuations observed on longer timescales. The increased amplitudes of brightness fluctuations on longer timescales are often described as the structure function, with the amplitude of fluctuation expressed by some measure such as rms deviation, as a function of the interval of time between successive samples of this fluctuating quantity.

Estimates of the structure function have been given for timescales of 1 day to years in Colley & Schild (1999, 2000), in a wavelet calculation and representation by Schild (1999), and also as a Fourier representation of the microlensing component (Schild 1996, Fig. 4; Thomson & Schild 1997). This last reference considers only fluctuations on long timescales, approximately 100 days, and is not considered further here. In the direct structure function estimates of CS03 and Colley & Schild (2000), the variance quantity plotted is the square of the brightness difference amplitude as a function of lag between brightness samples. Thus, for the plotted fit in Figure 6 of Colley & Schild (2000), the mean fluctuation amplitude for 1 day lag is 0.0063 mag, and the square root of the variance is proportional to the lag. In other words, the mean brightness increase, expressed as an rms, is a linear function of lag time.

The same information has been gleaned from a wavelet analysis of the A and B image brightness records as described in Schild (1999). There we report in Figures 5 and 6 the wavelet amplitude expressed as a mean absolute deviation, and in Figures 7 and 8 the amplitude expressed as an rms deviation, which is comparable to the presentation in Colley & Schild (2000). The results agree well, with the rms deviation extrapolated to a 1 day lag of 0.005 mag, and a linear trend of rms deviation increasing with lag for lags up to approximately 20 days. This linear increase in the structure function is significant and has never been interpreted in the context of a physical process, probably because it has heretofore been anomalous and unexpected. Standard accretion disk models would adopt a simple picture that a disturbance in the accretion disk limited by the causality principle, with the amount of the brightness change increasing with time as the disturbance spreads, would produce a structure function that increases with the square of the timescale for an optically thick accretion disk for which the observed optical disturbance increases as the area within causality, or as the cube for the optically thin case.

The observed linear increase is, however, compatible with the MECO quasar model discussed in § 7, in which the emitting source is seen as an "annular band" around the equator of the compact object, with the band "thickness" or cross-section diameter of 5.4×10^{14} cm, as estimated above. As the disturbance propagates along the length of the band, the causally connected luminosity increases linearly. However, note that the linear increase should end when the entire length is in causal connection; this occurs when light has traveled a distance of 30 proper lt-days, the ring diameter, corresponding to an elapsed time of 14 lt-days (in the observer's frame) when allowance is made for cosmological effects (the $[1 + z]$ correction to time) and for geometric effects related to the orientation of the quasar. Thus, the "events" seen in wavelet representation would produce up to 16 day wavelets. This 16 day limit may be present in the measured wavelet amplitudes, as in Figures 5–8 of Schild (1999), where we see that the linear trend for 2, 4, and 8 day wavelets curves toward a shallower slope in passing to 16, 32, and 64 day wavelets.

The upward trend of amplitude for image B wavelets at 64 days probably results from the microlensing events predicted by the SV03 model to relate to the luminous quasar Elvis outer structures. Thus, we conclude that both the basic timescale found for rapid quasar variability and the linear increase according to the measured structure function seem to favor an origin in an inner band–like MECO ring with approximately the theoretically expected thickness and radius.

5. TIMESCALES FOR QUASAR FUELING EVENTS ASSOCIATED WITH UNIT MASS INGESTION

Fundamental to the understanding of the quasar luminosity as a response to fueling must be an analysis of timescales associated with the fueling process. We begin with some comments about the nature of mass condensations in the universe.

A fundamental precept of the modern astrophysical view is that the universe is dominated by a nonbaryonic cold dark matter (CDM), which seeded and developed all structure observed today. We consider the arguments for the existence of this component weak, because the matter has not been found in laboratories despite 15 years of very determined searches, because observations of the low-redshift (local) universe do not find the expected substructure (Putman & Moore 2002), and because observations at the highest redshifts at which galaxies and quasars are observed do not conform to predictions. In particular, at redshifts 4–5, fully assembled galaxies with $10^9\,M_{\odot}$ are found far in excess of simulations, and the clustering of quasars and galaxies at redshifts 3–5 is much stronger than simulated in all CDM simulations. Worse, the high-redshift galaxies and quasars are observed to have solar metal abundances, even though the epoch of maximum star formation is expected to be between redshift 1 and 2. And contrary to the CDM theory, dwarf galaxies do not have the cusplike central structure expected (Spekkens et al. 2005).

The available simulations and theory consistently conclude that on spatial and mass scales relevant for quasar fueling structure in

the CDM distribution would be unimportant. A possible exception is the report by Diemand et al. (2005), which states that CDM clustering on planetary-mass scales is observed in simulations for axion CDM.

For the remainder of this paper, we adopt the point of view that CDM probably is too diffuse to contribute significantly to the fueling of quasars by discrete mass units. On the other hand, baryonic dark matter is now known to be significantly aggregated as condensations on specific scales. Stars seem to be in evidence everywhere, and their mass is probably reasonably taken to be in a lognormal distribution with a most probable value of 0.5 $M_{\odot}$ and a half-width of a factor of 10 around this most probable value (note that for a lognormal distribution, the mean, mode, and median are not the same, unlike the commonly accepted result for Gaussian statistics). Baryonic dark matter has been identified from quasar microlensing as a vast network of "rogue planets" having planetary mass and populating interstellar space everywhere (Schild 1996, 2005a).

A hydrodynamic theory that predicts this population (Gibson 1996)[5] as "primordial fog particles" ascribes their origin to fossil fluctuations pervading the universe and forming planetary-mass condensations at the time of recombination, 380,000 yr after the big bang. Since their discovery and interpretation from quasar microlensing, they are now being seen in quasar "extreme scattering events" (Walker & Wardle 1998; Wardle & Walker 1999) and in "pulsar scintillation scattering" events (Hill et al. 2004). The same hydrodynamic theory that predicts the formation of the primordial fog particles (Gibson 1996) also predicts that nature aggregated matter at the time of recombination in globular cluster mass scales, $10^6\ M_{\odot}$. These would be the objects mysteriously appearing on short timescales by the thousands during galaxy-galaxy collisions. Nearly all theories of structure formation acknowledge this "Jeans mass" scale of expected structure formation at recombination. This leaves us with a picture of baryonic dark matter with only a small fraction in smoothly distributed gas form and, more importantly, aggregated on scales of planets, stars, and globular clusters. Thus, we accept these as the unit fueling components for quasars.

The quasar response to this fueling process, seen as brightness fluctuations, has been summarized by de Vries et al. (2005) and summarized as a structure function in their Figure 8, where we see peaks of heightened brightness variability at timescales of 0.8 and 9 yr (in the quasar rest frame). The 0.8 yr feature is particularly well seen in their Figure 14 for events in their lower luminosity sample (*dark gray pentagons*) at a high level of significance. We consider that structure function analysis is a poor way to study the 0.8 yr fluctuations, and that wavelet analysis as applied to the Q0957+561 brightness statistics by Schild (1999) would be more suitable.

The 9 yr events are considered somewhat uncertain by de Vries et al. (2005) because of problems combining data sets related to different timescales. The structure function for more rapid variability in the Q0957+561 quasar has already been discussed in § 3. Of course, we now seek to match up the de Vries et al. (2005) structure function peaks with the fuel units, and we start by associating the 0.8 yr (300 day) events with primordial fog particle fueling. De Vries et al. (2005) stressed that these events are asymmetrical, typically having a slower rise time and more rapid decay and often but not always accompanied by a color shift toward blue. Typical events of this kind can be seen in the individual brightness curves from Giveon et al. (1999), who also referenced extensive earlier literature, and Hawkins (1996).

[5] Gibson (1996) is also available in electonic form as astro-ph/9904260.

Typical events have amplitude 0.3 mag and timescales (in the quasar rest frame) of approximately 300 days. These typical events have also been seen in the Q0957+561 brightness record, in which the $(1 + z)$ cosmological redshift expands the expected 300 day timescale to approximately 700 days. In the image A (less sensitive to microlensing) brightness record shown as Figure 1 in Pelt et al. (1998), three such events are seen peaking at JD $-$ 2,440,000 $=$ 5800, 7700, and 10,100. Observed amplitudes average approximately 0.25 mag. Thus, these Q0957+561 peaks are typical of the unit fueling events seen in all quasars. However, further structure in the Q0957+561 brightness history within one of these de Vries et al. "events" has been interpreted by SV03 as resulting from internal quasar structure on lags (observer's clock) of 125, 190, 540, and 625 days. Thus, for Q0957+561 the general peak in the de Vries structure function curve includes some component from internal quasar structure.

Since de Vries et al.'s (2005) work implies that high-luminosity quasars vary less than low-luminosity quasars, this result implies a quasar fueling scenario in which (1) variations have a limited absolute magnitude and (2) variations in luminosity are due to unit fueling events involving subcomponents or accretion instead of coherent variations of the quasar (de Vries et al. 2005). In this context we are now in a position to picture the quasar response to a typical unit fueling event. The event has an asymmetrical profile, with a rise time approximately twice as long as the decay time. During the event, the luminous quasar output increased approximately 30% in UV photons. Since the UV emission is found at nearly the center of the quasar's output spectrum we estimate from this that the quasar total output also increased by approximately 30%.

The average quasar luminosity fluctuation is observed to be on the order of 1×10^{44} ergs s^{-1}, over a 300 day duration. If this luminosity fluctuation is interpreted as being due to the integrated response to a unit planetoid-mass ingestion in the disk, then the total integrated energy associated with this process is 3×10^{51} ergs.

Since the unit-mass planetoid infall into the quasar accretion disk occurs from large distances, the total energy that contributes to the quasar disk luminosity on impact is equal to its relativistic kinetic energy times an efficiency factor, which is estimated to vary between 1% and 10%. Since the rest-mass energy of a $1 \times 10^{-3}\ M_{\odot}$ primordial planetoid is comparable to the total integrated energy of the 300 day quasar luminosity fluctuation, this luminosity fluctuation event can be plausibly interpreted as being caused by a collision of the quasar accretion disk with an infalling planetoid with mass on the order of this size that is moving relativistically. In this context the unit fueling process in quasars can be explained energetically in terms of primordial $1 \times 10^{-3}\ M_{\odot}$ planet-like particles infalling from large distances where the energy conversion to UV luminosity does not need to be very efficient.

This unit quasar-fueling mass, on the order of $1 \times 10^{-3}\ M_{\odot}$, is somewhat larger than the $1 \times 10^{-5}\ M_{\odot}$ unit mass that was previously inferred from quasar microlensing considerations (Schild 1996). However, we do not see this as a contradiction because the microlensing process responds to the particles with the largest optical depth, or to the peak of the mass distribution of the microlensing particles, which is on the order of $1 \times 10^{-5}\ M_{\odot}$. On the other hand, the size of the unit-mass ingestion associated with the quasar luminosity fluctuation process tends to select the more massive $1 \times 10^{-3}\ M_{\odot}$ particles in the primordial planetoid distribution, since the less massive infalling particles cause smaller fluctuations not seen in the brightness records.

Since in our scenario the 300 day events found by de Vries et al. (2005) and earlier authors are attributable to planetary-mass ingestion events, this allows us to make a falsifiable prediction.

The structure function analysis presented by de Vries et al. is not optimal for studying the nature of the 300 day events because either positive (brightening) or negative (fading) events could be responsible. However, our scenario predicts dominant positive events, and a more optimum analysis with wavelets as demonstrated by Schild (1999) would discriminate. Our unit fueling scenario predicts that the 300 day events should be dominated by positive (brightening) wavelets, and wavelet analysis would allow easily interpreted discrimination.

6. RADIO PROPERTIES OF Q0957+561 MEASURED BY MICROLENSING

In this section we analyze data for the Fourier power of the A and B quasar images and conclude that the B image shows more power at microlensing frequencies. From this and calculation of the coherence between the radio fluctuations seen, we are able to conclude that the radio-emitting region undergoes microlensing at radio frequencies. When we estimate the observed amplitude of the measured microlensing, we conclude that only a small fraction of the observed radio brightness from the identified region is microlensed in the observed radio microlensing events.

6.1. *The Coherence and Radio Brightness Imply Microlensing*

Radio emission at 6 cm has been monitored since the 1979 discovery of the Q0957+561 quasar by the MIT radio group (Lehar et al. 1992; Haarsma et al. 1997, 1999). The purpose was to determine the time delay, and in general one observation per month was made. At its high ecliptic latitude, Q0957+561 is far from the Sun on any calendar date, and the observing record is of high quality without the annual dropouts characteristic of optical data.

The basic process is revealed in the Fourier power spectrum for the 6 cm radio emission measured at the Very Large Array. Comparison of the A and B image power spectra shows extremely similar spectra from 0 to 3 cycles yr^{-1}, which relates to variability on timescales longer than 120 days. But a factor of 5 larger power level is seen for image B relative to A between 3 and 5 cycles yr^{-1}. Since the radio flux was sampled monthly, the sample frequency is 12 cycles yr^{-1} and the Nyquist frequency is 6 cycles yr^{-1}, or 60 days. However, inspection of the brightness record shows the existence of many brightness spikes indicated by two or more observations measured with the 30 day basic sampling rate, and thus, many individual events having a barely resolved 60 day timescale. Because the B image is seen through the lens galaxy, its optical depth to microlensing is higher than that of A. So if a stronger pattern of fluctuations is seen, it is interpreted as arising in microlensing. In other words, the A and B images are of the same quasar; so insofar as their brightness fluctuations differ, we attribute the difference to the microlensing that originates in the lens galaxy. It would be strongest in image B, which is seen through the lens galaxy and has a 4 times higher optical depth to microlensing by the granular structure of matter (stars, planets) in the lens galaxy.

If the higher amplitude of fluctuations limited to 3.5–5 cycles yr^{-1} is caused by microlensing, then there must be more spatial structure in the source or more microlensing particles of appropriate mass for 3.5–5 cycles yr^{-1}. The SV03 paper shows that solar-mass microlenses can produce cusps on this timescale, for the adopted standard transverse velocity of the cusp pattern. However, for microlensing to occur, both the fine cusps due to the granularity of the mass distribution in the lens galaxy *and* fine structure in the radio emission region must be present. This allows us to make size estimates for the radio-emitting region. The brightness fluctuations measured as power in Fourier spectral estimates on timescales of 3–5 cycles yr^{-1} are best seen in the brightness curves given in Haarsma et al. (1999, Fig. 4). We interpret the solid curves in the plot as showing the smoothed brightness trend of the two quasar images, and we find many pairs of points that reveal brightness spikes relative to the smoothed trend line. These spikes we interpret as microlensing events, and we find that they have typical brightness amplitudes of 5% on the required timescale, 60 days. Typical events in the B image record are seen at JD $- 2{,}440{,}000 = 6600$, 7600, 7700, 9400, 9600, and perhaps 10,300. It may also be seen that these events are more commonly seen in the B image than in A, confirming the result of the Fourier power spectrum estimate described above.

Again referring to the SV03 paper, at optical wavelengths it was estimated from direct simulation that structure on the scale of 2×10^{16} cm produces fluctuations on timescales of 150 days. Thus, we conclude from simple scaling arguments that the emitting radio source has a radius of approximately 2.2×10^{16} cm for an adopted mean microlensing particle mass of 0.5 $M_{\odot}$ (Schild 1996) and for the adopted event duration of 60 days.

6.2. *The Microlensed Fraction of* 6 cm *Radio Emission*

For structure on such scales, the R/R_0 test of Refsdal & Stabell (1991, 1993, 1997) cannot be applied because the size of the Einstein ring for a 0.5 $M_{\odot}$ star, 2×10^{16} cm, is comparable to the size of the emitting region, as estimated above. Thus, the small amplitude of the observed 60 day brightness fluctuations is not indicative of a very large source but rather is indicative that the microlensed source contains only a small fraction of the radio luminosity, as we now estimate.

The amplitude of radio brightness microlensing fluctuations has not yet been estimated by wavelet analysis as the optical has (Schild 1999). However, we easily estimate the amplitudes of some typical cusp-shaped events seen in the published radio brightness history (Haarsma et al. 1997, Fig. 4). Here we see that the strongly microlensed B image has typical event amplitudes of 1.4 mJy relative to the mean 25 mJy flux, or approximately 5% microlensing amplitude. Similarly, the A image has 1.9 mJy amplitude relative to a 35 mJy mean, or 5% amplitude. Because microlensing of a very compact source would produce events with amplitudes of a factor of 10 or 20, we immediately conclude that the radio source component with radius estimate 2.2×10^{16} cm contributes only a small fraction, approximately a percent, of the total measured 6 cm radio brightness.

It is further inferred that the remaining 99% of the measured 6 cm flux originates in a region too large to have microlensing events on timescales of 30 days to 10 yr, as has been previously inferred. The rapid small brightness fluctuations have sometimes been interpreted in the context of interstellar scintillations (Winn et al. 2004; Koopmans et al. 2003). We consider that the conclusion that, over the 3–5 cycles yr^{-1} microlensing frequency band centered at approximately 60 days, the Fourier power measured in the radio brightness curves is higher in the B image than in the A image in approximately the same ratio as the microlensing probability is a strong indication that the fluctuations originate in microlensing.

The position of the microlensed radio core source along the jet axis is also defined observationally. The radio and optical brightness have been found to have a substantial coherence with a lag of 35 days, with the optical preceding the radio (Thomson & Schild 1997). Thus, apart from geometric factors, the microlensed radio emitting region lies $35/(1 + z)$ lt-days above the inner quasar accretion disk structure, or 14.5 lt-days (3.6×10^{16} cm) above the central source (in projection). With correction for the calculated 54° inclination of the quasar's rotation axis with respect to the

line of sight, the compact microlensed radio emitting region is 9×10^{16} cm above the plane of the accretion disk. We conclude that a microlensed compact region of radio emission, contributing only a percent of the total radio flux, with a 2×10^{16} cm radius, is located 9×10^{16} cm above the accretion disk plane.

6.3. *Dynamic Origin of the Microlensed Radio Structure in Q0957+561 based on MECO Magnetic Field Line Reconnection Processes*

Recently the case of radio jet formation from a rotating collapsed object with an intrinsic magnetic dipole field aligned along the rotation axis was studied (Romanova et al. 2004). In that paper it was shown that such a configuration would produce a tangled network of magnetic field lines leading to the creation of magnetic towers associated with vertical quasi-periodic outflows. For the case of the central MECO in the quasar Q0957+561, we expect that an analogous type of stretching, bunching, breaking, and reconnection of the MECO magnetic field lines should occur at distances comparable to the sizes of the interior quasar SV03 structure radio structure discussed above.

When such reconnection effects act on the MECO magnetic field lines, the process is likely to entail their breaking and reconnection at the local Alfvén speed. Since the local Alfvén speed is relativistic in close proximity to the rotating central MECO object, we expect that the field line reconnection process described above has the potential to create the relativistic motions observed in radio jets.

The relativistic Alfvén speed is

$$v_{\rm A}^2 = \frac{c^2 B^2/4\pi}{\rho c^2 + \gamma P/(\gamma - 1) + B^2/4\pi}. \qquad (1)$$

In the MECO model in the low hard state (LHS), hot plasma containing magnetic field lines is quasi-periodically peeled off the inner magnetospheric radius of the accretion disk in the form of a funnel flow process similar to that described in Romanova et al. (2004). In the process of entering the magnetosphere, the poloidal magnetic field components are wound toroidally until $B^2/4\pi \approx \rho v_{\rm K}^2$, where $v_{\rm K} \sim 0.2c$ is the Keplerian speed of the inner disk.

At the inner disk radius $\gamma \sim 5/3$, and the gas pressure P, which essentially matches the magnetic pressure of the poloidal field component at the edge of the inner disk, is negligible by the time the base of the jet is reached. For this reason, in the toroidally wound donut that falls in through the magnetosphere, the gas pressure P is negligible. The end result of this fact is that $B^2/4\pi \sim \rho c^2$ near the base of the jet.

The energy density required for plasma to escape from deep inside the gravitational well is about $GM\rho/r_e$, where r_e is the "ejection radius." At this radius, the energy density of the wound-up toroidal magnetic field in the donut is $B_\phi^2/4\pi$, and this is what drives the jet. Equating these energy densities leads to $r_e \sim 4\pi GM\rho/B_\phi^2 = GM/v_{\rm A}^2$. Taking $r_e = 2 \times 10^{16}$ cm from the observed Schild-Vakulik structure leads to the result that $v_{\rm A} = 0.16c$; hence the Alfvén speed associated with this process near the MECO is relativistic.

7. THEORETICAL ANALYSIS AND OVERVIEW OF THE SCHILD-VAKULIK STRUCTURE INSIDE QUASAR Q0957+561

In this section we discuss the applicability of currently known theoretical quasar models to the empirical Schild-Vakulik (SV03) structure discussed in the preceding sections. Based on our observational evidence, Q0957+561 has structural elements as follows (see Fig. 1):

Elliptical Elvis coronal structure: $R_e = 2 \times 10^{17}$ cm, $H_e = 5 \times 10^{16}$ cm.

Inner radius of accretion disk: $R_m = 74R_g = 3.9 \times 10^{16}$ cm.

Size of hot inner accretion disk annulus: $\delta(R_m) = 5.4 \times 10^{14}$ cm $= 1R_g$.

Size and location of base of radio structure: $R_r = 2 \times 10^{16}$ cm, $H_r = 9 \times 10^{16}$ cm.

Note that some of the dimensions listed above related to the sizes of the optical structures differ by factors of roughly 2 from the values stated in the SV03 paper. This is because the projection angle deduced in Schild (2005b) implies projection factors that make the Figure 1 sideways-viewed quantities larger by about that factor. Our quoted dimensions in the bottom part of Table 2 correspond to the dimensions shown in Figure 1.

The radial width of the UV-luminous Elvis structure, δR_e was estimated in SV03 to be 2×10^{16} cm and was estimated from microlensing of the broad emission lines by Richards et al. (2004) to be a comparable 1.4×10^{16} cm. Since the quasar Q0957+561 has been observed to contain a central compact object with a mass on the order of $M = (3\text{–}4) \times 10^9\ M_\odot$, the observed SV03 structure inner accretion disk radius of 3.9×10^{16} cm implies that the inner radius of the accretion disk is located at about $74R_g$. In addition, at this radius a hot annulus of material exists with a radial thickness of 5.4×10^{14} cm (which for the above mass is on the order of $1R_g$ in radial thickness). Finally, the hyperbolic Elvis coronal structure, which is observed in Q0957+561, appears, on the basis of its observed H_r/R_r ratio, to have a rather wide opening angle of 76° with respect to the z-axis of rotation.

At first, one might consider explaining the SV03 structure in terms of intrinsic magnetic moment generated by a central spinning charged black hole in the quasar Q0957+561. However, this explanation fails because the necessary charge on the spinning black hole required to make it work would not be stable enough to account for the long lifetime of the SV03 structure. This inherent instability occurs because the value of the charge-to-mass ratios of electrons and protons implies that opposing electric forces on them would then be at least an order of magnitude larger than their gravitational attraction to the central black hole. In addition, it would be difficult to maintain this required charge on the spinning black hole if it were also surrounded by an accretion disk like that observed in quasar Q0957+561.

Since Q0957+561 appears to be in a radio-loud LHS with a very large $74R_g$ inner accretion disk radius, a second method to explain the above observations would be to use a standard Kerr black hole–advection dominated accretion flows (ADAF)–accretion disk–jet model (Narayan & Quataert 2005). One would do this by choosing the parameters in this scenario so that the transition from the hot thin outer disk to the inner ADAF disk occurs at the $74R_g$ radius. However since the magnetic field in this model is anchored to the accretion disk and not to the central Kerr black hole, this model cannot account for either the very thin $1R_g$ radial size of the observed hot inner accretion disk annulus at the $74R_g$ radius, or the wide Elvis outflow opening angle of 76° with respect to the z-axis of rotation (since the frame dragging on the disk magnetic field that occurs in Kerr black hole–ADAF–accretion disk–jet models characteristically generates jetlike outflows with relatively narrow opening angles on the order of 30° with respect to the z-axis of rotation; e.g., see Fig. 1 of the Narayan & Quataert 2005).

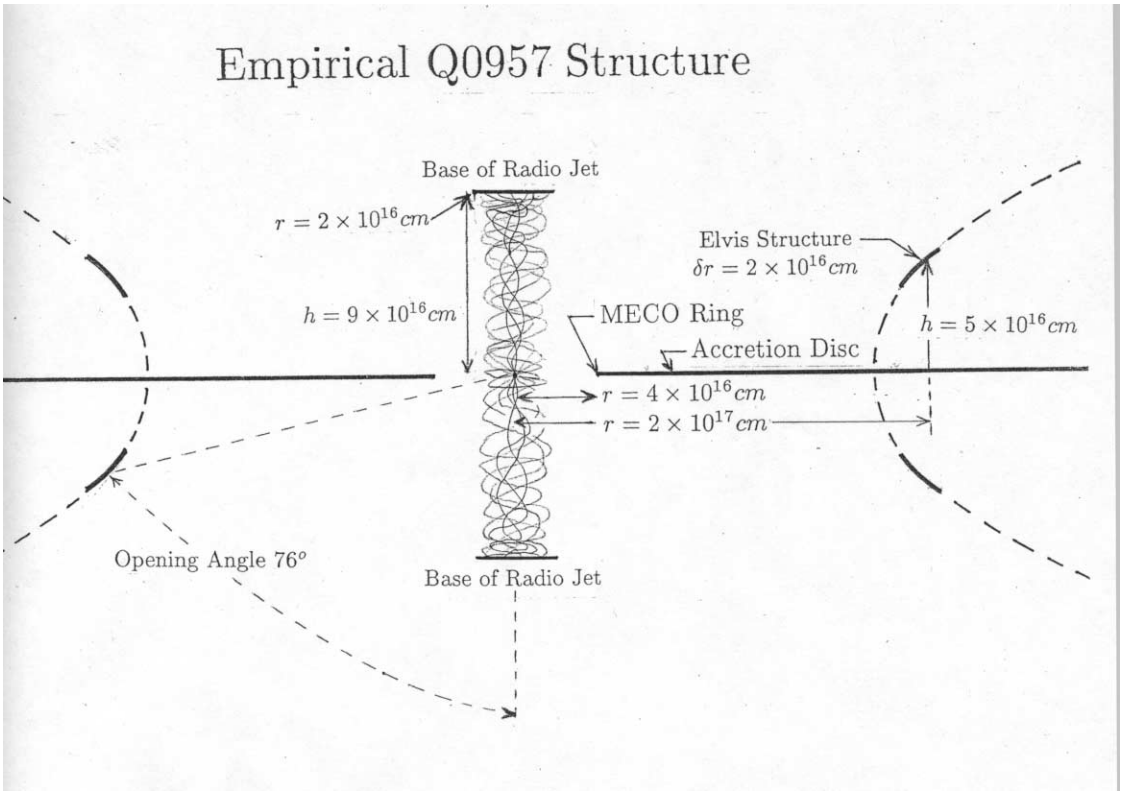

FIG. 1.— Cartoon showing the principal structures in the empirical quasar model and specifying the size scales of the structures found, expressed in centimeters. In this cross-sectional view, the outer Elvis outflow structures must be understood as a section of the surfaces of revolution, and the luminous portions are shown as solid line segments. These have been modeled as circles in the SV03 simulations. The inner luminous edge of the accretion disk, marked "MECO Ring," has a very high surface brightness and is found to be outside an unexpectedly large empty inner region. The tangled magnetic field lines are shown only to the base of the radio jet. The overall geometry and proportions correspond closely to the rotating magnetic star models of Romanova et al. (2002, 2003a).

Since the standard black hole–ADAF–accretion disk–jet model does not predict the SV03 structure correctly, a third and final attempt to find a black hole description for the SV03 structure observed in Q0957+561 would be to apply the MAD black hole model (Igumenschev et al. 2003) to the above described structure. In this case MAD parameters would be chosen that would set the magnetospheric radius of the MAD accretion disk at $74R_g$. However, in this MAD model description of Q0957+561, instead of the observed hot annular band of material of radial thickness on the order of $1R_g$, there would now occur at this radius a stochastic injection of hot blobs of plasma that would orbit into the black hole while emitting visible radiation from $74R_g$ all the way down to the photon orbit at $3R_g$. Based on the Keplerian orbital periods at $74R_g$, the MAD black hole model would then generate observable periodic luminosity fluctuations whose local periods at the quasar, over the radial interval ranging from $74R_g$ down to the photon orbit at $3R_g$, would be on the order of 800 days. Hence, if this MAD black hole model had been operating in Q0957+561, the clean fluctuation signal associated with the inner hot ring structure of the Schild-Vakulik model would not have been seen because of the smearing out of all of the MAD quasi-periodic oscillations that would be occurring in the orbital range from $74R_g$ down to $3R_g$. Furthermore, periodic brightness fluctuations produced by luminous hot blobs crossing caustics created by the complex mass distribution in lens galaxy G1 would produce highly periodic (approximately 100 day) brightness spikes, which were not observed.

Hence, we find that neither spinning charged black holes, the standard black hole–ADAF–accretion disk–jet model, nor the MAD black hole model (the latter two of which contain magnetic fields that are assumed to be anchored in the accretion disk and not anchored to the central compact black hole object) can account for all four of the components of SV03 structure observed within the quasar Q0957+561.

Having tried all of the plausible black hole models and finding them unsatisfactory, we now show that the four components of the Schild-Vakulik structure in the quasar Q0957+561 can be consistently described within the context of the MECO model (Robertson & Leiter 2002, 2003, 2004, 2005; Leiter & Robertson 2003), in which a very strong intrinsic magnetic field anchored to a slowly rotating, highly redshifted central compact MECO object interacts in a magnetic propeller mode with the surrounding accretion disk and generates the four components of the SV03 structure with Elvis coronal outflows that can have a wide opening angle greater that 60° with respect to the z-axis of rotation.

The formal details about the MECO model that appear in the above papers have been summarized into a series of short appendices (Appendices 1–11 in Schild et al. [2005]) for the convenience of the reader and are referred to in the following sections as needed in order to clarify the details of specific calculations. More specific information and simulations for the magnetic propeller mode of central compact magnetic objects surrounded by accretion disks can be found in Romanova et al. (2002, 2003a).

We begin our MECO analysis of the SV03 structure in Q0957+561 starting with Table 1 below, in which column (1) summarizes the MECO physical quantities relevant to Q0957+561 and the location in the appendices in Schild et al. (2005) where, for the convenience of the reader, the associated derivations and discussions about these physical quantities can be found; column (2) gives the specific form of the equations to be used in the calculation of these physical quantities, and column (3) gives the functional form of

TABLE 1
MASS SCALING EQUATIONS ASSOCIATED WITH A VERY HIGH REDSHIFT EDDINGTON-LIMITED MECO

MECO Physical Quantity (1)	Equation (2)	Mass Scaling (3)
Surface redshift (App. 1, 9–10)	$1 + z_s = 1.5 \times 10^8 (M/7)^{1/2}$	$M^{1/2}$
Surface luminosity (observed) (App. 5)	$L_s = L_{\rm Edd}/(1 + z_s)$ ergs s^{-1}	$M^{1/2}$
Surface temperature (observed) (App. 5)	$T_s = 2.3 \times 10^7/[M(1 + z_s)]^{1/4}$ K	$M^{-3/8}$
Rotation rate (App. 7)	$\nu_2 = 0.89\left(L_{q,32}/M\right)^{0.763}/L_{c,36}$ Hz	M^{-1}
Quiescent luminosity (App. 7)	$L_{q,32} = 0.65M\left(L_{c,36}/M\right)^{1.75}$ ergs s^{-1}	M
Corotation radius (App. 7)	$R_c = 46.7R_g/\left(M\nu_2\right)^{2/3}$ cm	M
Magnetosphere radius (App. 7)	$R_m = 3.33R_g\left[\mu_{27}^4/(L_{\rm X}/L_{\rm Edd})^2 M^{10}\right]^{1/7}$ cm	M
Magnetic moment (App. 7)	$\mu_{27} = 8.16\left(L_{c,36}M/\nu_2^3\right)^{1/2}$ cm	$M^{5/2}$
Magnetic field (App. 7)	$B_{\theta,10} = 1.12(R_g/r)^3[L_{c,36}/(M^5\nu_2^3)]^{1/2}$ G	$M^{-1/2}$
Radio luminosity (App. 8)	$L_{\rm rad,36} = 10^{-6.635}M^{0.835}L_{\rm X,36}^{2/3}[1 - (L_{\rm X,36}/L_{c,36})^{1/3}]$ ergs s^{-1}	$M^{3/2}$

NOTE.—This table references the appendices to Schild et al. (2005).

the relevant mass scaling of these physical quantities in order to demonstrate clearly how the equations for these physical quantities can be applied to the case of both GBHCs and AGNs.

Then, (1) assuming that the MECO behavior of this quasar in the radio-loud LHS is similar to that of an average MECO-GBHC in the radio-loud LHS (like that analyzed in the Robertson-Leiter papers discussed above) and (2) using the observed values of X-ray luminosity, radio luminosity, redshift ($z = 1.4$), and the physical dimensions of the internal SV03 structure for Q0957+561 as input in the mass-scaled MECO equations in Table 1, then (3) the results shown in Table 2 are obtained.

Table 2 is intended to be read as follows: in the top part, the scaling relations from Table 1 and other input data are used to determine the properties of the GBHC and AGN. In the bottom part, the empirical size scale parameters determined by Schild & Vakulik and corrected for the specific quasar orientation factors in Schild (2005b) are scaled and tabulated for the GBHC case according to our adopted scaling relations.

In this manner we found that the presence of a $3.6 \times 10^9\ M_\odot$ MECO acting as the central compact object in the quasar Q0957+561 consistently predicted all of the four components of the observed SV03 structure. The physical picture that emerged was as follows: (1) Since Q0957+561 is a radio-loud quasar in a LHS, the inner region of the MECO accretion disk at the magnetospheric radius R_m is larger than the corotation radius R_c, and the nonthermal MECO-LHS X-ray emission is generated by the magnetic propeller interaction of the intrinsic magnetic moment in the central MECO with the inner accretion disk. (2) The line driving force generated within the radiation field environment around the MECO, acting in conjunction with the MECO intrinsic magnetic propeller interaction with the accretion disk and the magnetic corona about it, then acts to generate the hyperbolic Elvis outflow of plasma with the wide opening angle observed at 2×10^{17} cm from the central object as well as leading to the development of a radio jet. This radio emission structure has radius R_r of 2×10^{16} cm and height H_r of 9×10^{16} cm above the accretion disk plane (Fig. 1). (3) The inner region of the accretion disk is located at $R_m = 1.4R_c$, where R_m is the magnetospheric radius, and the MECO corotation radius R_c is $53R_g$. A high-density, optically thick, radially thin inner band of material of radial thickness δR_m given by $0.014R_m$ and equal to 5.4×10^{14} cm is formed by the MECO magnetic propeller at the magnetospheric radius R_m. The thermal emission from this hot optically thick inner band then accounts for the observed small blue thermal UV bump and its microlensing fluctuations. Normalizing the optically thick MECO accretion disk to that of a neutron star–X-ray binary, we find that the temperature T_t of the thermal emissions from the thin hot inner annulus of material at radius R_m is 7200 K. For the observed Q0957+561 redshift of $z = 1.4$, this thin hot inner annulus generates the observed local thermal "little blue bump" emission at wavelength 2700 Å with a thermal UV luminosity L_t equal to 1.4×10^{44} ergs s^{-1} (which is equal to about one-quarter of the total UV luminosity generated by Compton upscattering from the larger hyperbolic Elvis coronal structure, also present).

Hence in the context of the MECO model we have shown that the quasar Q0957+561 in a radio-loud LHS is physically similar to a mass-scaled-up version of an average MECO-GBHC where, because of the cooler accretion disk that occurs in the quasar, all four components of the SV03 structure are observable. The basic observable elements of the SV03 structure in this quasar are (1) a large Elvis elliptical coronal structure with a 76° opening angle with respect to the z-axis of rotation, (2) a large magnetospherically generated inner accretion disk radius, (3) a thin hot inner accretion disk annulus located at the magnetospheric radius, and (4) a radio structure whose base is located directly above the central MECO.

We have demonstrated that the MECO model is able to explain all of the properties of the SV03 structure observed in the quasar Q0957 as intrinsic magnetic propeller interactions with the accretion disk. Hence, on this basis we conclude that the presence of the SV03 structure represents observable evidence for the existence of an intrinsic magnetic moment generated by a central MECO in the heart of this quasar.

8. CONCLUSIONS

We have examined the empirical data for the lensed and microlensed Q0957+561 A and B quasar obtained from 20 years of brightness monitoring at visible wavelengths (near-ultraviolet emission at the quasar). We have also examined several conclusions inferred previously from analysis of the autocorrelation and microlensing properties of the monitoring data, and we have now collected these results in a consistent presentation that can confront physical quasar models and their simulations.

The structures and luminosities found, referred to as the Schild-Vakulik structure (SV03 structure), are associated with a bright inner edge of the accretion disk, surrounded by a coronal outflow (Elvis structure) long known to explain the complex spectroscopic behavior observed in quasars. However, it is observed that the opening angle of the coronal Elvis structure with respect to the z-axis of rotation appears to have a very large value of 76°. In addition, a radio emission region has been located directly above the compact source. In particular, the size and location of this

TABLE 2
MASS SCALING OF LHS MECO-GBHC TO QUASAR Q0957

Parameter	Average MECO-GBHC	MECO-Quasar Q0957
MECO Physical Quantities		
Mass of central MECO	$7\ M_\odot$	$3.6 \times 10^9\ M_\odot$
Surface redshift	1.5×10^8	3.4×10^{12}
Surface luminosity (distantly observed)	6.1×10^{30} ergs s^{-1}	1.4×10^{35} ergs s^{-1}
Surface temp (distantly observed)	1.3×10^5 K	69 K
Rotation rate	12 Hz	2.3×10^{-8} Hz
Intrinsic magnetic moment	2.1×10^{30} G cm^3	1.2×10^{52} G cm^3
Magnetic field (distantly observed)	$(8.3 \times 10^9$ G$)\ (6Rg/r)^3$	$(3.6 \times 10^5$ G$)\ (6Rg/r)^3$
Quiescent X-ray luminosity	2×10^{33} ergs s^{-1}	9.4×10^{41} ergs s^{-1}
Corotation radius	$53R_g$	$53R_g$
X-ray luminosity	4.7×10^{36} ergs s^{-1}	2.4×10^{45} ergs s^{-1}
Radio luminosity	1.1×10^{30} ergs s^{-1}	1.3×10^{43} ergs s^{-1}
Schild-Vakulik Structures		
Magnetosphere radius	$R_m = 74R_g = 7.6 \times 10^7$ cm	$R_m = 74R_g = 4 \times 10^{16}$ cm
Hot inner disk band	$\delta(R) = R_g = 10^6$ cm	$\delta(R) = Rg = 5.4 \times 10^{14}$ cm
Base of radio jet	$R_r = 5 \times 10^7$ cm, $H = 2 \times 10^8$ cm	$R_r = 2 \times 10^{16}$ cm, $H = 9 \times 10^{16}$ cm
Elvis corona[a]	$R_e = 5 \times 10^8$ cm, $H = 1.2 \times 10^8$ cm	$R_e = 2 \times 10^{17}$ cm, $H = 5 \times 10^{16}$ cm

[a] Elvis coronal structure may not be seen in hot LHS MECO-BGBHC accretion disks.

radio-emitting region have been found to correspond to where the reconnection of magnetic field lines at relativistic Alfvén speeds, like that generated by a rotating central object containing an intrinsic magnetic field, should occur.

Although our data do not include near-infrared data related to the dusty torus, the standard picture now shows that this torus structure lies 20% farther from the central source than the Elvis outflow structures, and is thus presumably in a velocity dead zone shielded by the Elvis outflow. Note that Suganuma et al. (2004) show in their Table 2 that for Seyfert galaxy NGC 5548, the highest excitation lines of hydrogen and O III lie closest to the central source, with the low excitation lines of O I and Mg II twice as far out, and the K-band infrared emission 20% farther out still. It is difficult to imagine that the infrared-emitting dust particles could survive the intense X-ray and ultraviolet fluxes originating at the central source, and it is most likely that the dusty torus lies in the equatorial region sheltered by the Elvis outflow structures.

In the discussion in § 7 we showed that attempts to model the observations of the SV03 structure in the quasar Q0957+561 in terms of an intrinsic magnetic moment generated by a central spinning charged black hole failed because the necessary charge on the spinning black hole required to make it work would not be stable enough to account for the long lifetime of the SV03 structure. Similarly, attempts to model the SV03 structure in terms of the class of Kerr black hole–ADAF–accretion disk corona–jet models, in which the magnetic field is intrinsic to the accretion disk and not the central rotating black hole, were shown to have difficulty in that they were unable to account for the very large opening angles that are observed for the coronal Elvis outflows. Finally, we showed that magnetically arrested disk black hole models also have problems in that they predict the existence of orbiting infalling hot blobs of plasma inside the inner region of the accretion disk that are not observed.

On the other hand, we have found that the SV03 empirical structure can be successfully explained by magnetospheric eternally collapsing object (MECO) models, which feature a highly redshifted, Eddington-limited, collapsing central compact object containing a strong intrinsic magnetic field aligned with the MECO axis of rotation. In this model the resulting MECO magnetic propeller effects that interact with the inner regions of the accretion disk create an inner luminous annular (bandlike) structure and an outer coronal structure characterized by strong relativistic outflow with a wide opening angle to the z-axis of rotation as is observed in the SV03 empirical structure. In particular, the size and location of the radio-emitting region associated with the SV03 structure in the quasar Q0957+561 have been found to correspond to the region above the central compact object where the reconnection of magnetic field lines at relativistic Alfvén speeds, like that generated by a rotating central MECO containing an intrinsic magnetic field, should occur.

The MECO contains a central rotating magnetic object whose dynamo sweeps clean the central region of the quasar out to a distance at which the magnetic propeller acts on the inner edge of the accretion disk and a radio-emitting region above the disk where magnetic field lines must twist and bunch up until they eventually break and reconnect at relativistic speeds. Such an object does not have an event horizon; instead, infalling material collects at an inner structure just beyond $2R_g$ that further collapses to higher redshift while remaining in causal connection for all time. Because of the small light cone angle for radiation escaping from this highly redshifted region to the distant observer, the resulting low luminosity in the far-infrared wavelengths makes this region difficult to detect in the case of quasar Q0957+561.

It is important to note that the MECO model that seems to best fit the empirical SV03 structure in the quasar Q0957+561 differs significantly from most black hole models currently under consideration. In particular, the predicted SV03 empirical structures they generate seem to resemble the complex inflow-outflow pattern seen in magnetic propeller models for young stellar objects. The action of such magnetic propeller forces has been discussed and simulated by Romanova et al. (2003a, 2003b, 2004) with nonrelativistic models that produce observable structures that are closely similar to the observed Schild-Vakulik structure.

We have also found that the MECO explanation of the empirical SV03 structure implies an interesting similarity between the MECO model for the quasar Q0957+561 and the MECO

models that explain the phenomena associated with Galactic black hole candidates in the LHS with luminosity on the order of 1/10 of a percent of the Eddington-limit luminosity.

On the basis of the above observational and theoretical arguments we conclude that the observation of the Schild-Vakulik structure in the quasar Q0957+561 represents strong evidence for the existence of an observable intrinsic magnetic moment, generated by a supermassive $3.6 \times 10^9\ M_\odot$ MECO acting as the central compact object in this active galaxy, which implies that this quasar does not have an event horizon.

APPENDIX A

MAGNETOSPHERIC ETERNALLY COLLAPSING OBJECTS (MECOs)

Using the Einstein-Maxwell equations and quantum electrodynamics in the context of general relativistic plasma astrophysics, it has been shown (Schild et al. 2005) that it is possible to virtually stop and maintain a slow, steady (on the order of many Hubble times!), secular collapse of a compact physical plasma object outside of its Schwarzschild radius with photon pressure generated by synchrotron radiation from an equipartition surface magnetic field. To control the rate of collapse, the object must radiate at the local Eddington limit but from a highly redshifted surface.

Referring to Appendices 9 and 10 of Schild et al. (2005a), we have shown that surface drift currents within a pair plasma at the MECO surface can be shown to be able to generate the required fields. Drift currents proportional to $\boldsymbol{g} \times \boldsymbol{B}/B^2$ occur for plasmas at rest in gravitational and magnetic fields. The equatorial poloidal magnetic field associated with an Eddington-limited secular rate of collapse of the highly redshifted exterior surface of the MECO can be shown to be controlled by quantum electrodynamic pair production processes which can occur in strong magnetic fields on the order of $\sim 10^{20}$ G. Magnetic fields of this magnitude are strong enough to create a redshift-dependent source of bound electron-positron pairs in the plasma at the surface of the MECO (in addition to the copious production of electron-positron pairs created by photon-photon collisions in the highly compact pair-dominated plasma in the MECO), whose interaction with the Eddington-limited synchrotron radiation acts to stabilize the secular collapse rate. The magnetic field of the interior is approximately what one would expect from flux compression during collapse, $\sim 2.5 \times 10^{13} (7\ M_\odot/M)^{1/2}$ G, and its radial component is continuous across the surface boundary. The poloidal field is discontinuous across the surface and much stronger externally due to the surface drift currents. As shown in Appendix 9 of Schild et al. (2005a), at the MECO surface radius R_s (which is slightly larger than the Schwarzschild radius $2GM/c^2$), the ratio of the poloidal field on the surface to the poloidal field just under the MECO surface is given by

$$B_{\theta,S^+}/B_{\theta,S^-} = (1+z_s)/[2\ln(1+z_s)] = 10^{20}/(2.5 \times 10^{13})\sqrt{7\ M_\odot/M}, \quad (2)$$

where z_s is the surface redshift. This has the solution

$$1 + z_s = 1.5 \times 10^8 \sqrt{M/7\ M_\odot}. \quad (3)$$

The $\sim 10^{20}$ G poloidal magnetic field on the surface of the MECO generates an intrinsic magnetic moment, which when distantly observed is reduced by a factor of $3(1+z_s) = 4.5 \times 10^8 (M/7\ M_\odot)^{1/2}$ due to the surface redshift of the MECO, to a level that agrees well with the intrinsic magnetic moments observed in GBHCs and AGNs. The surface luminosity is also reduced below the conventional Newtonian Eddington limit by $(1+z_s)$ when distantly observed, and the decay lifetime is extended by the same factor. Figure 2 represents a schematic diagram summarizing the physical mechanisms contributing to the creation of a MECO in the general relativistic gravitational collapse process, which is discussed in Appendices 1–11 of the longer Schild et al. (2005) version of this paper.

APPENDIX B

ON THE BLACK HOLE KERR-SCHILD METRIC AND MECO VAIDYA METRIC SOLUTIONS TO THE GRAVITATIONAL COLLAPSE PROBLEM

In discussions with experts in general relativity the validity of our motivation to look for physical alternatives to black holes has been questioned. Our work has been based on the assumption that the preservation of the SPOE in nature implies that metrics with event horizons are nonphysical. The objection to this has been based on the well-known fact that for massive particles under the action of both gravitational and nongravitational forces, the timelike nature of the world line of massive particles is preserved. The generally covariant equation of motion for their timelike world lines in spacetime is given by

$$Du^\mu/d\tau = a^\mu = K^\mu. \quad (4)$$

Here u^μ is the 4-velocity of the massive particle and K^μ is the generally covariant nongravitational 4-vector force that in general relativity is required to obey the dynamic condition

$$K^\mu a_\mu = 0. \quad (5)$$

Then, from the above two equations it follows that

$$D(u^\mu u_\mu)/d\tau = 0, \quad (6)$$

which guarantees that (where we have chosen units in which $c = 1$ and use the spacetime metric signature $[1, -1, -1, -1]$)

$$u^\mu u_\mu = 1. \quad (7)$$

From this it follows that in general relativity the timelike invariance of the worldline of a massive particle is dynamically preserved for all metric solutions, $g_{\mu\nu}$, to the Einstein equations, including the case of the "event horizon penetrating" Kerr-Schild metric used by most black hole theoreticians in computer simulations of the black hole collapse of a radially infalling massive particle or fluid. On the basis of the above facts it is then argued that there is no reason to look for physical alternatives to black holes and that the assumption that the preservation of the SPOE in nature implies that metrics with event horizons are nonphysical is in error.

However, we now show that the above arguments, which are based on the 4-velocity u^μ alone, are not valid. This is because relativitists who come to this conclusion in this manner are making the mistake of ignoring the fact that in addition to the 4-velocity u^μ there exists another important quantity called the physical 3-velocity that must be considered as well. Physically speaking, the magnitude of the physical 3-velocity is seen by an observer at rest as being equal to the speed of the comoving observer who is moving along with the collapsing massive particle or fluid. If we consider the case of a radially infalling massive particle or fluid

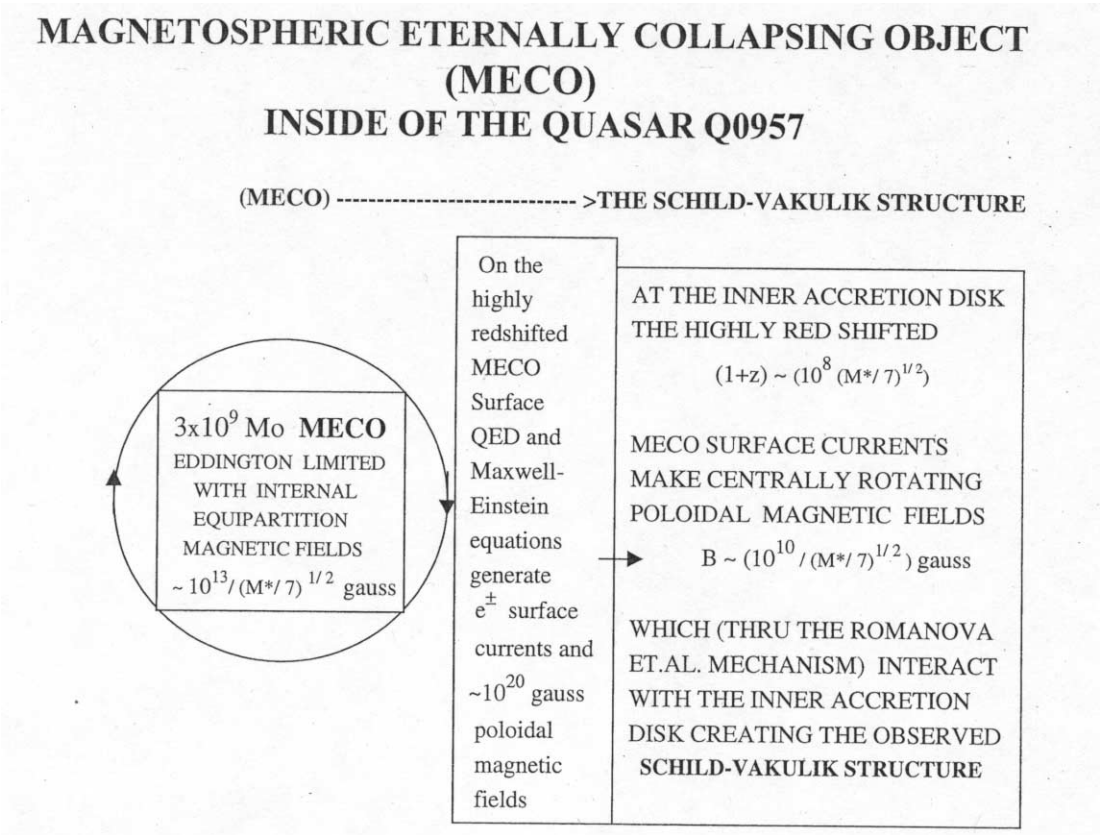

FIG. 2.— Logic diagram showing how the MECO picture of physical quasar structure has been applied to the empirical quasar structure picture of SV03. The rotating central object with Eddington-limited internal equipartition magnetic fields generates surface currents and rotating poloidal magnetic fields that clear out the inner quasar region. The central rotating fields in the LHS interact with the inner edge of the accretion disk to produce the high surface brightness band at the inner accretion disk edge. The magnetic fields operating through the coronal region through the Romanova et al. (2002, 2003a) interaction create the outer Elvis outflow structures simulated in SV03.

undergoing gravitational collapse, it can be shown that the radial component of the physical 3-velocity is given by

$$V^r = c\frac{[(g_{0r}g_{0r} - g_{rr}g_{00})v^r v^r]^{1/2}}{|(g_{00} + g_{0r}v^r)|}, \qquad (8)$$

where $v^r = dr/d\tau$ is the radial coordinate velocity of the massive particle of fluid (see Landau & Lifshitz 1975, pp. 248–252).

From the above formula for the radial component of the physical 3-velocity of the comoving observer V^r we see that for metrics that have the property that $g_{00} \rightarrow 0$ in some region of spacetime (i.e., the property associated with the existence of an event horizon for the nonrotating metrics associated with the radial infall of matter), the physical radial velocity V^r of the comoving frame of the massive particle or fluid becomes equal to the speed of light as the massive particle or fluid crosses the event horizon.

Hence, even though the timelike property $u^\mu u_\mu = 1$ is preserved for a massive particle or fluid crossing the event horizon of the Kerr-Schild metric where $g_{00} \rightarrow 0$ occurs, a local special relativistic connection between the comoving frame of the radially infalling massive particle or fluid and a stationary observer can no longer be made. Since the SPOE requires that special relativity must hold locally at all points in spacetime, the breakdown at the event horizon of the local special relativistic connection between the comoving observer frame and a stationary observer frame for a particle crossing the event horizon represents a violation of the SPOE. Hence, we have shown that by considering both the 4-velocity and the physical 3-velocity of the comoving observer there is motivation to look for physical alternatives to black holes. In fact, in this context logical arguments can be consistently made that show that black holes with nonzero mass cannot exist in nature (Mitra 2000, 2002, 2006a, 2006b).

Based on the above arguments, the SPOE-preserving requirement that the comoving observer frame for a massive collapsing fluid must always be able to be connected to a stationary observer by special relativistic transformations with a physical 3-speed that is less than the speed of light was taken seriously in our work. In the literature the requirement that the SPOE must be preserved everywhere in spacetime for the timelike worldlines of massive particles or fluids under the influence of both gravitational and nongravitational forces goes under the technical name of "timelike worldline completeness."

Based on this idea we have found that preservation of the SPOE in nature can be accomplished only if there exist nongravitational components in the energy-momentum tensor on the right-hand side of the Einstein equation that physically guarantee the preservation of the SPOE. It was in this alternative context that the general relativistic MECO solutions to the Einstein-Maxwell equations emerged, as was shown in the three previously published papers of Robertson & Leiter and developed in more detail in Appendices 1–10 of Schild et al. (2005). There it was shown that for a collapsing body, the structure and radiation transfer properties of the energy-momentum tensor on the right-hand side of the Einstein field equations could describe a collapsing radiating object that contained equipartition magnetic fields that generated a highly redshifted Eddington-limited secular collapse process.

This collapse process was shown to satisfy the SPOE requirement of timelike worldline completeness by dynamically preventing trapped surfaces, which lead to event horizons, from forming.

More specifically in Appendices 1–10 of Schild et al. (2005) it was shown that, by using the Einstein-Maxwell equations and QED in the context of general relativistic plasma astrophysics, it was possible to virtually stop and maintain a slow (many Hubble times), steady collapse of a compact physical plasma object outside of its Schwarzschild radius. The nongravitational force is Compton photon pressure generated by synchrotron radiation from an intrinsic equipartition magnetic dipole field contained within the compact object. The rate of collapse is controlled by radiation at the local Eddington limit, but from a highly redshifted surface. In Appendices 9 and 10 of Schild et al. (2005) it was shown that general relativistic surface drift currents within a pair plasma at the MECO surface can generate the required magnetic fields. In Appendix 9 the equatorial poloidal magnetic field associated with a locally Eddington-limited secular rate of collapse of the exterior surface was shown to be strong enough to spontaneously create bound electron-positron pairs in the surface plasma of the MECO. In the context of the MECO highly redshifted Eddington-limited balance, the action of this QED process was shown to be sufficient to stabilize the collapse rate of the MECO surface.

For the case of hot collapsing radiating matter associated with the MECO, the corresponding exterior solution to the Einstein equation was shown to be described by the time-dependent Vaidya metric. No coordinate transformation between the MECO Vaidya metric and the black hole Kerr-Schild metric exists. Since the highly redshifted MECO Vaidya metric solutions preserve the SPOE and do not have event horizons, they can also contain a slowly rotating intrinsic magnetic dipole moment. These magnetic moments have observable effects if such MECOs exist at the centers of GBHCs and AGNs. In support of this idea our paper contains observational evidence that the physical effects of such intrinsic magnetic dipole fields in the central compact object in the quasar Q0957+561 have been seen. It is important to note that the physical effects of the MECO intrinsic magnetic dipole fields that our observations have found in the quasar Q0957+561 cannot be explained in terms of standard black hole models using Kerr-Schild metric–driven general relativistic magnetohydrodynamics calculations, since these calculations generate unphysical split magnetic monopole fields that cannot explain the details of the intrinsic structure in Q0957+561 that our observations have found.

We reiterate that the Kerr-Schild metric used by most relativitists is not relevant to the work done in this paper, because the collapsing radiating MECO solution to the Einstein equation is described by the time-dependent radiating Vaidya metric, and there is no coordinate transformation between them. Thus, while we did not lightly ignore the Kerr-Schild metric as applied to standard black hole solutions of the Einstein field equations, our approach instead was to start with the gravitational microlensing and nanolensing observations of the quasar Q0957+561, which seemed to show the physical effects of an intrinsic dipole magnetic field attached to the collapsed slowly rotating central compact object, which the Kerr-Schild metric solutions did not allow. Therefore, we found that we had to turn to alternate MECO Vaidya metric solutions to the Einstein-Maxwell equations, which feature the intrinsic magnetic dipole fields implied by the observations.

REFERENCES

Colley, W., & Schild, R. 1999, ApJ, 518, 153
———. 2000, ApJ, 540, 104
———. 2003, ApJ, 594, 97 (CS03)
Colley, W., et al. 2003, ApJ, 587, 71
de Vries, W. H., Becker, R. H., White, R. L., & Loomis, C. 2005, AJ, 129, 615
Diemand, J., Moore, B., & Stadel, J. 2005, Nature, 433, 389
Elvis, M. 2000, ApJ, 545, 63
Gibson, C. 1996, Appl. Mech. Rev., 49, 299
Giveon, U., Maoz, D., Kaspi, S., Netzer, H., & Smith, P. S. 1999, MNRAS, 306, 637
Gould, A., & Miralde-Escude, J. 1997, ApJ, 483, L13
Haarsma, D., Hewitt, J. N., Lehar, J., & Burke, B. F. 1997, ApJ, 479, 102
———. 1999, ApJ, 510, 64
Hawkins, M. 1996, MNRAS, 278, 787
Hill, A., Stinebring, D. R., Asplund, C. T., Berwick, D. E., Everett, W. B., & Hinkel, N. R. 2005, ApJ, 619, L171
Igumenschev, I., Narayan, R., & Abramowicz, M. 2003, ApJ, 592, 1042
Koopmans, L., et al. 2003, ApJ, 595, 712
Landau, L. D., & Lifshitz, E. M. 1975, Classical Theory of Fields (4th ed.; Oxford: Pergamon Press)
Lehar, J., Hewitt, J. N., Burke, B. F., & Roberts, D. H. 1992, ApJ, 384, 453
Leiter, D., & Robertson, S. 2003, Found. Phys. Lett., 16, 143
Mitra, A. 2000, Found. Phys. Lett., 13, 543
———. 2002, Found. Phys. Lett., 15, 439
———. 2006a, in Proc. 29th Int. Cosmic Ray Conference (India), in press (astro-ph/0507697)
———. 2006b, in Focus on Black Hole Research, ed. P. V. Kreitler (Hauppage: Nova Science), in press
Narayan, R., & Quataert, E. 2005, Science, 307, 77
Oscoz, A., et al. 2001, ApJ, 552, 81
Pelt, J., Kayser, R., Refsdal, S., & Schramm, T. 1996, A&A, 305, 97
Pelt, J., Schild, R., Refsdal, S., & Stabell, R. 1998, A&A, 336, 829
Pijpers, F. 1997, MNRAS, 289, 933
Press, W., Rybicki, G. B., & Hewitt, J. N. 1992, ApJ, 385, 404
Putman, M., & Moore, B. 2002, in ASP Conf. Proc. 254, Extragalactic Gas at Low Redshift, ed. J. Mulchaey & J. Stocke (San Francisco: ASP), 245
Rauch, K., & Blandford, R. 1991, ApJ, 381, 39
Refsdal, S., & Stabell, R. 1991, A&A, 250, 62
Refsdal, S., & Stabell, R. 1993, A&A, 278, L5
———. 1997, A&A, 325, 877
Richards, G., et al. 2004, ApJ, 610, 679
Robertson, S., & Leiter, D. 2002, ApJ, 565, 447
———. 2003, ApJ, 596, L203
———. 2004, MNRAS, 350, 1391
———. 2005, in New Directions in Black Hole Research, ed. P. V. Kreitler (Hauppauge: Nova Science), 1
Romanova, M. M., Toropina, O. D., Toropin, Yu. M., & Lovelace, R. V. E. 2003a, ApJ, 588, 400
Romanova, M. M., Ustyugova, G. V., Koldoba, A. V., & Lovelace, R. V. E. 2002, ApJ, 578, 420
———. 2004, ApJ, 616, L151
Romanova, M. M., Ustyugova, G. V., Koldoba, A. V., Wick, J. V., & Lovelace, R. V. E. 2003b, ApJ, 595, 1009
Schild, R. 1990, AJ, 100, 1771
———. 1996, ApJ, 464, 125
———. 1999, ApJ, 514, 598
———. 2005a, in Proc. Fifth International Workshop on the Identification of Dark Matter, ed. N Spooner & V. Kudryavtsev (London: World Scientific), 183
———. 2005b, AJ, 129, 1225
Schild, R. E., Leiter, D. J., & Robertson, S. L. 2005, preprint (astro-ph/5055518)
Schild, R. & Thompson, D. J. 1997a, AJ, 113, 130
———. 1997b, in Astronomical Time Series, ed. D. Maoz, A. Sternberg, & E. Liebowitz (Dordrecht: Kluwer), 73
Schild, R. E., & Vakulik, V. 2003, AJ, 126, 689 (SV03)
Spekkens, K, Giovanelli, R., & Haynes, M. 2005, AJ, 129, 2119
Suganuma, M., et al. 2004, ApJ, 612, L113
Thomson, D. J., & Schild, R. 1997, in Applications of Time Series Analysis in Astronomy and Meteorology, ed. T. Subba Rao, M. Priestly, & O. Lessi (New York: Chapman & Hall), 187
Vakulik, V., Schild, R., Dudinov, V., Nuritdinov, S., Tsvetkova, V., Burkhonov, O., & Akhunov, T. 2006, A&A, 447, 905
Walker, M., & Wardle, M. 1998, ApJ, 498, L125
Wardle, M., & Walker, M. 1999, ApJ, 527, L109
Winn, J., et al. 2004, AJ, 128, 2696
Wyithe, S., Webster, R., & Turner, E. 2000, MNRAS, 318, 1120